

High-performance of ultra-low Pt loading PEMFCs: carbon-encapsulated CoFe alloy supported Pt nanoparticles as high-efficiency electrocatalysts

Jingjing Zhang^a, Kechuang Wan^b, Xue Xu^d, Qiong Xue^a, Zhijia Jin^c, Zenghai Shan^a, Pingwen Ming^b, Jia Wang^{a,c,}, Bing Li^b and Cunman Zhang^{b,*}*

^a Shanghai XCMG Intelligent Technology Co., Ltd, Shanghai, 200063, China

^b Clean Energy Automotive Engineering Center & School of Automotive Studies, Tongji University, Shanghai 201804, China

^c School of Automotive Engineering, Changshu Institute of Technology, Jiangsu, 215500, China

^d Center for Excellence in Brain Science and Intelligence Technoloav. Chinese Academy of Sciences

*Corresponding author.

E-mail address: zhangcunman@tongji.edu.cn (C. M. Zhang), libing210@tongji.edu.cn (B. Li), 1911089@tongji.edu.cn (J. Wang)

1. Experimental Section

1.1 Preparation of the Catalyst

The synthesis procedures for the CoFe-NOC/Co-NOC/Fe-NOC were reported in our previous work. The Pt nanoparticles were dispersed CoFe-NOC/Co-NOC/Fe-NOC supports by a solvothermal method. The CoFe-NOC, Co-NOC, and Fe-NOC supports were first stirred and ultrasonically treated in a 0.1 M HNO₃ solution at 60 °C (aiming to remove unstable transition metals and enhance the stability of the supports), followed by washing with water and freeze-drying for storage. Next, The Pt(acac)₂ (25 mg) was ultrasonically dispersed in 30 mL of ethylene glycol solution, and after stirring for 1 hour, sodium citrate (400 mg) was added to the solution. After stirring for an additional hour, 3 mol/L KOH solution was added until the pH = 9. Subsequently, CoFe-NOC/Co-NOC/Fe-NOC (75 mg) support was added, and the mixture was stirred for 30 minutes, followed by 30 minutes of ultrasonication. The reaction was carried out in an oil bath at 180 °C under a nitrogen atmosphere for 4 hours. After cooling to room temperature, the mixture was centrifuged and washed with water and ethanol. Finally, the resulting catalyst was freeze-dried overnight to obtain Pt/CoFe-NOC, Pt/Co-NOC, and Pt/Fe-NOC catalysts.

1.2 Materials characterization

The morphologies of catalysts and the changes after the durability test were analyzed by transmission electron microscopy (TEM). The crystallinity of catalysts was determined by X-ray diffraction (XRD). Raman spectroscopy was employed to measure the graphitization degrees in carbon materials and analyze their structural changes. The bulk compositions of catalysts were characterized by inductively coupled plasma mass spectrometry (ICP-MS). Scanning electron microscopy (SEM) was

employed to analyze the sample shape of catalysts. The specific surface areas and pore size distributions of carbon supports were obtained by Brunauer–Emmett–Teller (BET) analysis with high-purity N₂ as filling gas after degassing at 200 °C for 8 h.

1.3 Fabrication of MEAs

The slurry was prepared by dispersing catalyst and 5% Nafion solution into water and isopropanol (volume ratio of 1:1). This slurry was sprayed onto a membrane of 25 cm² (GORE, thickness of 10 μm), and then the gas diffusion layers (25BC, SGL) were fixed to both sides of the as-sprayed membrane to produce MEAs. The MEAs were fabricated using the Pt/CoFe-NOC, Pt/Co-NOC, and Pt/Fe-NOC catalysts and the commercial 20wt% Pt/C(JM) catalyst in the cathode and anode, respectively, and two controls were obtained using Pt/CoFe-NOC, Pt/Co-NOC, and Pt/Fe-NOC in the cathode and only Pt/C (JM) in both electrodes. The Pt loadings of the cathode and anode in all of the MEAs are 0.05 and 0.1 mgPt cm⁻².

1.4 Electrochemical Evaluation

The electrochemical tests of supports and catalysts were conducted by a rotating disc electrode (RDE) technique. The catalyst of 2 mg was added to a Nafion/ethanol solution of 1 mL (the mass ratio of Nafion solution/ethanol is 1:30) to obtain the catalyst ink. Cyclic voltammetry (CV), linear sweep voltammetry (LSV), and 30000 cycles of durability testing (in 0.1M HClO₄ solution) were employed to estimate electrochemical activity and durability of catalysts.

1.5 Single-Cell and High Potential Durability Tests of MEAs

All MEAs performed the same single-cell tests. The operating conditions of polarization curves was as follows: the cell temperature, relative humidity (RH), back pressure (relative to the atmosphere), and H₂/air stoichiometric ratio (excess coefficient) are 80 °C, 100%, 150 kPa, and 1.7:3.0, respectively. The operating conditions of the durability test were as follows: the cell temperature and RH were 80 °C and 100%, respectively, and the cathode and anode were supplied with N₂ and H₂ of 0.2 NLPM.

1.6 Theoretical calculations

We employed Density Functional Theory (DFT) calculations to investigate the interactions between CoFe-NOC, Co-NOC, Fe-NOC supports and Pt. The aim is to compare the adsorption strengths of ORR reaction intermediates on different Pt-loaded supports. The calculations use the Generalized Gradient Approximation (GGA) with the Perdew-Burke-Ernzerhof (PBE) functional to describe electronic exchange and correlation effects. A plane-wave cutoff energy of 42 eV is applied, with a real-space separation of at least 15 Å. The convergence criteria for energy and force during the geometry optimization are set to 10^{-5} eV and -0.01 eV/Å, respectively. A $3 \times 3 \times 1$ Monkhorst-Pack k-point grid is used for sampling. Based on the models of Pt loaded on the three different supports, the d-band centers and electron transfer directions are calculated.

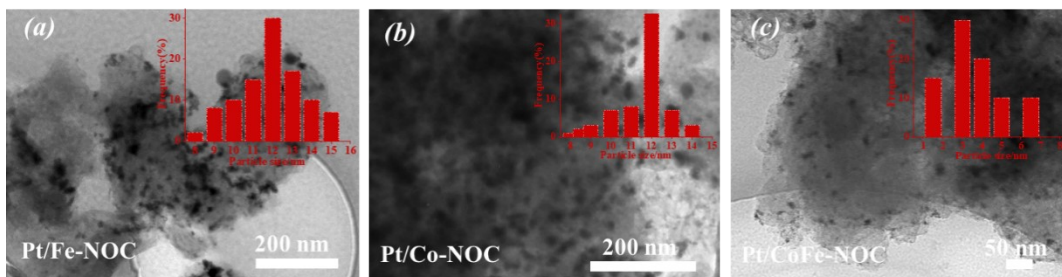


Figure S1. TEM images and particle size distributions of (a) Pt/Fe-NOC, (b) Pt/Co-NOC, (c) Pt/CoFe-NOC.

According to the EDS results, the Pt elements concentration is higher than that of Co and Fe, and this difference can be attributed to the multi-metallic synergistic effect on the dispersion and loading of platinum. In the Pt/CoFe-NOC system, the synergistic effect of Co and Fe optimizes the surface properties of the support, forming more favorable active sites for the anchoring of platinum nanoparticles. As a result, the Pt elements concentration is higher than the Co and Fe concentrations. Due to the limitations of EDS in determining metal concentrations, the X-ray signal from EDS primarily comes from the surface and shallow layers of the sample, with a typical detection depth of only a few micrometers. This means that if there is a difference in metal concentration between the surface and the interior of the sample, the EDS results can only represent the surface concentration, which may not accurately reflect the metal concentration throughout the entire material. In this paper, the Pt/CoFe-NOC sample, after nitric acid washing, removed unstable cobalt and iron metals, leaving mainly carbon-encapsulated cobalt and iron. This led to a significant deviation in determining the metal concentration based purely on EDS results. Therefore, we re-characterized the metal concentrations in the Pt/CoFe-NOC material using ICP-MS (Table S1), and the results showed that the platinum mass fraction reached 19.01 wt.%, while cobalt and iron mass fractions were 1.3 wt.% and 1.17 wt.%, respectively. Interestingly, the platinum mass fractions in the Pt/Co-NOC and Pt/Fe@-NOC samples were 16.6 wt.% and 17.5 wt.%, respectively. both lower than the platinum mass fraction in the Pt/CoFe-NOC material. This result validates our previous analysis that the bi-metallic (Co and Fe) support contains significantly more platinum loading sites than the single-metal

(Co/Fe) supports, which leads to a higher platinum mass fraction in the Pt/CoFe-NOC sample compared to the Pt/Co-NOC and Pt/Fe@-NOC samples.

催化剂	质量百分数		
	Pt wt.%	Co wt.%	Fe wt.%
Pt/CoFe-NOC	19.01	1.3	1.07
Pt/Co-NOC	16.6	1.3	/
Pt/Fe-NOC	17.5	/	1.07

Table S1. The Pt, Co and Fe mass loading of Pt/CoFe-NOC, Pt/Fe-NOC and Pt/Co-NOC.

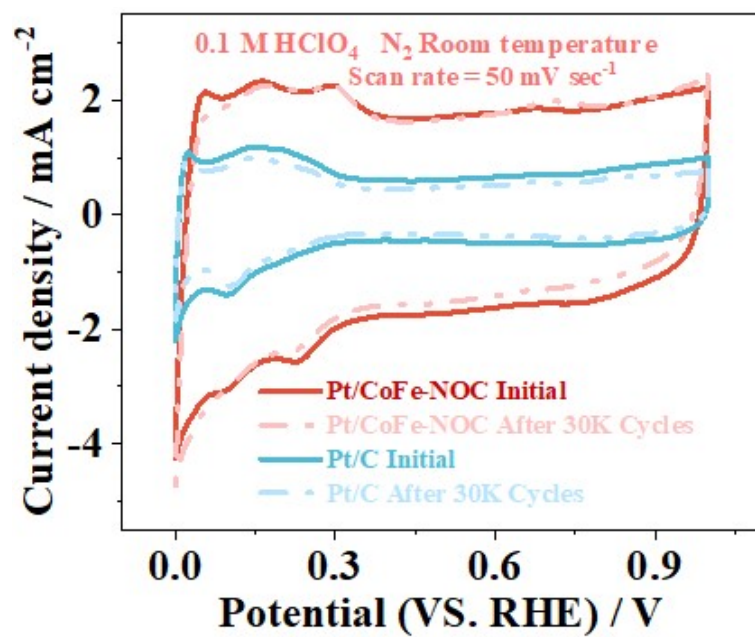


Figure S2. CV curves of Pt/CoFe-NOC and Pt/C catalysts before and after ORR stability tests.

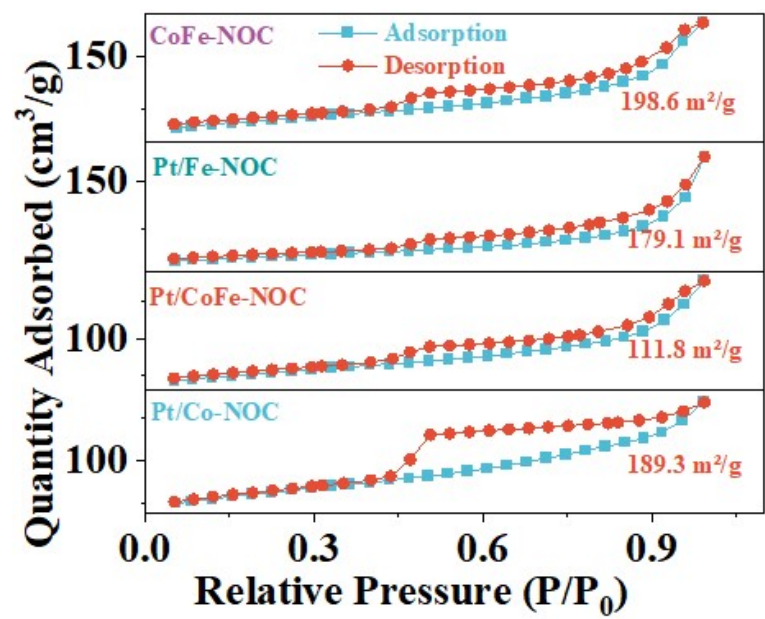


Figure S3. N₂ adsorption-desorption isotherms of CoFe-NOC, Pt/CoFe-NOC, Pt/Co-NOC and Pt/Fe-NOC catalysts.

Table S2. The peak position of Pt 4f and percentage (%) of Pt⁰ and Pt^{δ+} in Pt/CoFe-NOC, Pt/Co-NOC, and Pt/Fe-NOC.

		Pt_{NP}CoFe@NOC		Pt_{NP}Co@NOC		Pt_{NP}Fe@NOC	
Pt ⁰ 4f(eV)	7/2	70.5	15.2%	70.5	25.6%	70.5	28.0%
	5/2	73.9	32.3%	73.9	24.1%	73.9	21.6%
Pt ^{δ+} 4f(eV)	7/2	71.1	23.7%	71.1	32.0%	71.1	34.1%
	5/2	74.7	28.5%	74.7	18.2%	74.7	16.0%

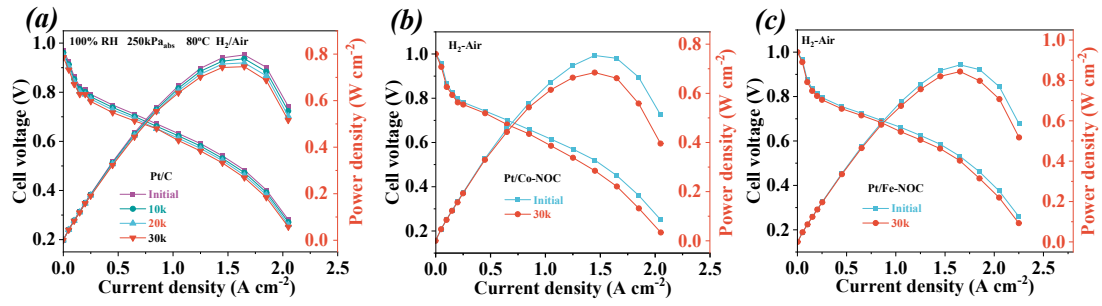


Figure S4. Polarisation curves and power density before and after stability tests. (a) Pt/C. (b) Pt/Co-NOC. (c) Pt/Fe-NOC.

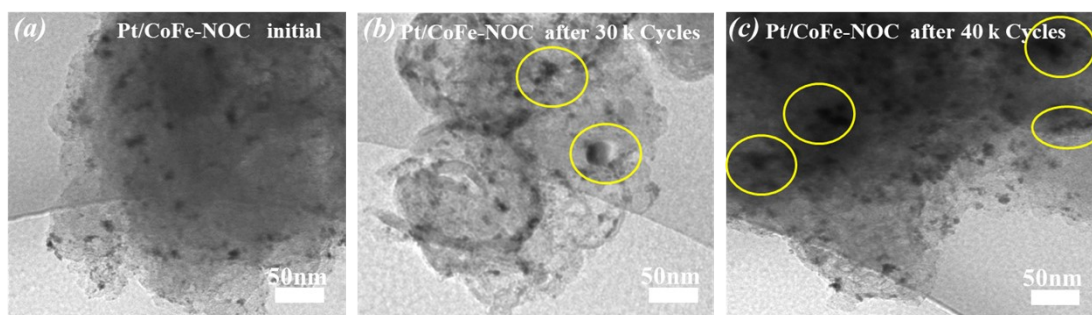


Figure S5. Comparison of TEM plots of Pt/CoFe-NOC catalyst before and after durability cycling.

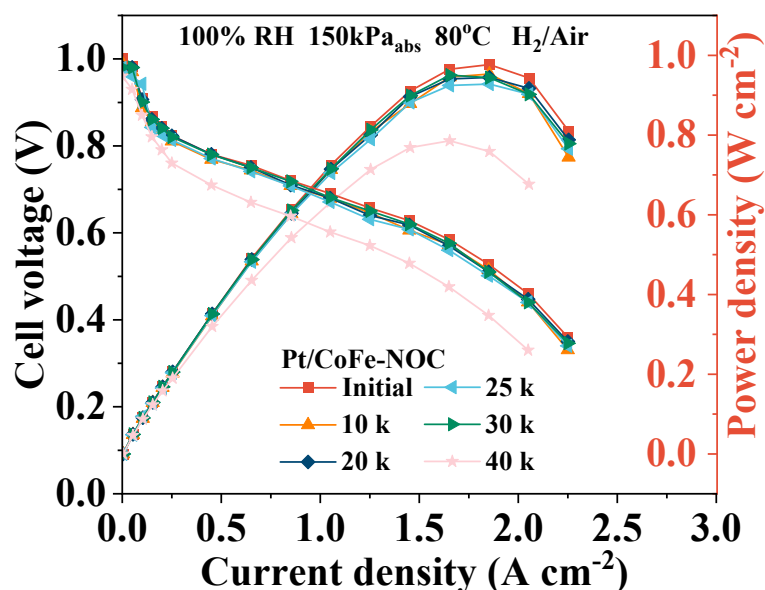


Figure S6. Polarisation curves and power density before and after stability tests. of Pt/CoFe-NOC catalysts.

we have conducted further evaluations on the stability of the MEA (Pt/CoFe-NOC) by extending the testing to 40,000 (40 k) cycles to assess the degradation of the Pt/CoFe-NOC catalyst. TEM images (Figure 10) reveal significant platinum particle aggregation (highlighted by yellow circles) after 40 k cycles, with some regions exhibiting Pt nanowires. Compared to the catalyst before testing and after 30 k cycles, the aggregation of Pt particles is more pronounced. The observed performance degradation after 40 k cycles is attributed to the aggregation of Pt nanoparticles. Thus, the low-Pt catalyst Pt/CoFe-NOC demonstrates a progressive increase in Pt nanoparticle aggregation as the testing duration extends.

Table S4. Fuel-cell performance for Pt/CoFe-NOC catalyst and the representative results from recent works.

Catalysts	Pt loading (mgPt cm⁻²) Anode/Cathode	Test condition	Durability (AST)	Peak power density (W.cm⁻²) Before and after cycles	Re.
PtCo@Gnp	0.01/0.09	H ₂ /O ₂	30000	1.0/0.79	[1]
PtCo/HSC-f	0.015/0.06	H ₂ /Air	30000	1.1/	[2]
i- CoPt@Pt/KB	0.1/0.1	H ₂ /O ₂	30000	1.2/1.0	[3]
Pt-700	0.1/0.2	H ₂ /O ₂	20000	0.96/0.84	[4]
PtCo/KB-NH ₂	0.1/0.2	H ₂ /Air	30000	1.19/0.96	[5]
L10-PtZn/Pt- C	0.1/0.104	H ₂ /Air	30000	0.8/0.78	[6]
Pt ₃ Co/FeN ₄ -C	0.1/0.1	H ₂ /Air	30000	0.92/0.83	[7]
Pt/C NMs	0.1/0.11	H ₂ /Air	30000	0.55/	[8]
Pt1Co1- IMC@Pt/C	0.1/0.2	H ₂ /Air	30000	1.25/1.1	[9]
Co-doped Pt/C	0.025/0.05	H ₂ /Air	30000	0.92/0.7	[10]
Pt/N-KB	0.15/0.105	H ₂ /O ₂	1500	1.3/	[11]
PtFe@FeSAs- N-C	0.2/0.12	H ₂ /Air	30000	0.71/	[12]
p-Pt/KB- NaOH	0.2/0.4	H ₂ /Air	100(h)	1.13/1.10	[13]
MSA-PtCo/C	0.025/0.1	H ₂ /Air	100(h)	1.05	[14]

Pt ₃ Co/Co-NC	0.1/0.1	H ₂ /Air	30000	0.84/0.79	[15]
PFPA-PIM-SBI	0.07	H ₂ /O ₂	720(h)	0.3	[16]
Pt/CoFe-NOC	0.05/0.1	H ₂ /Air	30000	0.97/0.95	This work
Pt/CoFe-NOC	0.05/0.1	H ₂ /Air	40000	0.97/0.79	This work

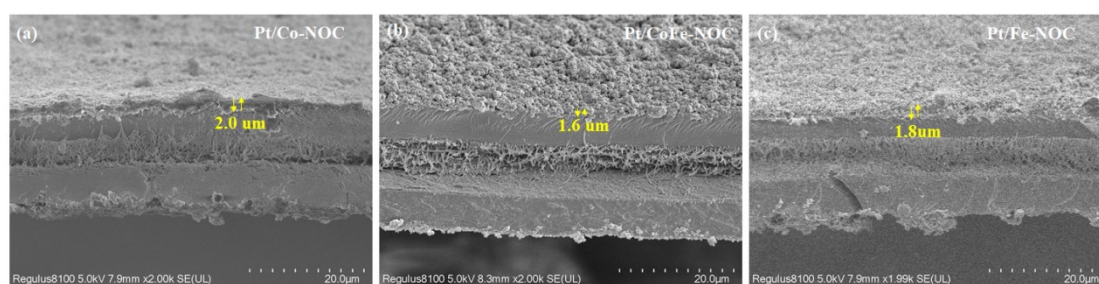


Figure S6. SEM images of MEA sections: (a) Pt/Co-NOC (b) Pt/CoFe-NOC and (c) Pt/CoFe-NOC.

Normalization is fundamental to the performance evaluation of low-platinum-loaded MEAs. In this paper, we have systematically normalized from two aspects: the platinum loading in the MEA and the platinum content measured by three-electrode testing, as shown in Figure 11. According to the ICP-MS results (Table 1), the mass percentage of Pt loaded on single-metal carriers is lower than that on bi-metal supports. Therefore, to ensure consistency in the platinum loading of the MEA, the resulting catalyst layer thickness of the fabricated MEA may vary (Figure 11). Specifically, Pt/Co-NOC and Pt/Fe-NOC materials have a lower platinum mass percentage, and their MEA catalyst layer thickness is greater than that of Pt/CoFe-NOC MEAs.

References

- [1] Zhao Z, Liu Z, Zhang A, Yan X, Xue W, Peng B, Xin H L, Pan X, Duan X, Huang Y. Graphene-nanopocket-encaged PtCo nanocatalysts for highly durable fuel cell operation under demanding ultralow-Pt-loading conditions [J]. *Nature Nanotechnology*, 2022, 17(9): 968-975.
- [2] Kongkanand, A. In highly-accessible catalysts for durable high-power performance, 2017 Annual Merit Review and Peer Evaluation Meeting, Washington, DC https://www.hydrogen.energy.gov/pdfs/review17/fc144_kongkanand, 2017.
- [3] Yoo T Y, Lee J, Kim S, Her M, Kim S-Y, Lee Y-H, Shin H, Jeong H, Sinha A K, Cho S-P, Sung Y-E, Hyeon T. Scalable production of an intermetallic Pt–Co electrocatalyst for high-power proton-exchange-membrane fuel cells [J]. *Energy & Environmental Science*, 2023, 16(3): 1146-1154.
- [4] Li Z, Zou J, Xi X, Fan P, Zhang Y, Peng Y, Banham D, Yang D, Dong A. Native Ligand Carbonization Renders Common Platinum Nanoparticles Highly Durable for Electrocatalytic Oxygen Reduction: Annealing Temperature Matters [J]. *Advanced Materials*, 2022, 34(26), 2202743.
- [5] Gong Q, Zhang H, Yu H, Jeon S, Ren Y, Yang Z, Sun C-J, Stach E A, Foucher A C, Yu Y, Smart M, Filippelli G M, Cullen D A, Liu P, Xie J. Amino-tethering synthesis strategy toward highly accessible sub-3-nm L10-PtM catalysts for high-power fuel cells [J]. *Matter*, 2023, 6(3): 963-982.
- [6] Liang J, Zhao Z, Li N, Wang X, Li S, Liu X, Wang T, Lu G, Wang D, Hwang B J, Huang Y, Su D, Li Q. Biaxial Strains Mediated Oxygen Reduction Electrocatalysis on Fenton Reaction Resistant L1₀-PtZn Fuel Cell Cathode [J]. *Advanced Energy Materials*, 2020, 10(29), 2000179.
- [7] Qiao Z, Wang C, Li C, Zeng Y, Hwang S, Li B, Karakalos S, Park J, Kropf A J, Wegener E C, Gong Q, Xu H, Wang G, Myers D J, Xie J, Spendelow J S, Wu G. Atomically dispersed single iron sites for promoting Pt and Pt₃Co fuel cell catalysts: performance and durability improvements [J]. *Energy & Environmental Science*, 2021, 14(9): 4948-4960.

- [8] Hu Y, Zhu M, Luo X, Wu G, Chao T, Qu Y, Zhou F, Sun R, Han X, Li H, Jiang B, Wu Y, Hong X. Coplanar Pt/C Nanomeshes with Ultrastable Oxygen Reduction Performance in Fuel Cells [J]. *Angewandte Chemie International Edition*, 2021, 60(12): 6533-6538.
- [9] Cheng Q, Yang S, Fu C, Zou L, Zou Z, Jiang Z, Zhang J, Yang H. High-loaded sub-6 nm Pt₁Co₁ intermetallic compounds with highly efficient performance expression in PEMFCs [J]. *Energy & Environmental Science*, 2022, 15(1): 278-286.
- [10] Duan X, Cao F, Ding R, Li X, Li Q, Aisha R, Zhang S, Hua K, Rui Z, Wu Y, Li J, Li A, Liu J. Cobalt-Doping Stabilized Active and Durable Sub-2 nm Pt Nanoclusters for Low-Pt-Loading PEMFC Cathode [J]. *Advanced Energy Materials*, 2022, 12(13), 2103144.
- [11] Ott S, Orfanidi A, Schmiehs H, Anke B, Nong H N, Hübner J, Gernert U, Glied M, Lerch M, Strasser P. Ionomer distribution control in porous carbon-supported catalyst layers for high-power and low Pt-loaded proton exchange membrane fuel cells [J]. *Nature Materials*, 2019, 19(1): 77-85.
- [12] Zhao L, Zhu Z, Wang J, Zuo J, Chen H, Qi X, Niu X, Chen J S, Wu R, Wei Z. Robust p-d Orbital Coupling in PtCoIn@Pt Core-Shell Catalysts for Durable Proton Exchange Membrane Fuel Cells [J]. *Angew Chem Int Ed Engl*, 2025, 64(19): 231-243.
- [13] Yang S, Shu Q, Fu B, Liu S, Zhang Y, Zhao H. Synthesis of high-performance low-Pt (1 1 1)-loading catalysts for ORR by interaction between solution and nonthermal plasma [J]. *Chemical Engineering Journal*, 2024, 488(12): 1231-1245.
- [14] Zhang L, Tong L, Li S, Ma C-S, Xue K-Z, Liang H-W. Synthesis of intermetallic PtCo fuel cell catalysts from bimetallic core@shell structured nanoparticles [J]. *Journal of Energy Chemistry*, 2025, 101(3): 1-6.
- [15] Luan S, Liu J, Li S, Li S, Lou Z, Lv M, Cui X, Jiang L. Unveiling the synergistic effect of metal/nitrogen-doped carbon and Pt₃Co nanoclusters for boosting the oxygen reduction reaction in PEMFC [J]. *Chemical Engineering Journal*, 2025,

503(3): 1311-1326.

- [16] Li H, Zuo P, Wu W, Tang G, Fang J, Xu T, Yang Z. Electrode binder design for high-power, low-Pt loading and durable high temperature fuel cells [J]. *Energy & Environmental Science*, 2024, 17(10): 3651-3659.